5-2020

Low Temperature Effects on the Mechanical, Fracture, and Dynamic Behavior of Carbon and E-glass Epoxy Laminates

James LeBlanc

Paul Cavallaro

Jahn Torres

David Ponte

Eric Warner

See next page for additional authors

Authors

James LeBlanc, Paul Cavallaro, Jahn Torres, David Ponte, Eric Warner, Ryan Saenger, Irine Neba Mforsoh, and Aun Shukla

International Journal of Lightweight Materials and Manufacture 3 (2020) 344–356

Contents lists available at ScienceDirect

International Journal of Lightweight Materials and Manufacture

journal homepage: https://www.sciencedirect.com/journal/international-journal-of-lightweight-materials-and-manufacture

Original Article

Low temperature effects on the mechanical, fracture, and dynamic behavior of carbon and E-glass epoxy laminates

James LeBlanc [a, *], Paul Cavallaro [a], Jahn Torres [a], David Ponte [a], Eric Warner [a], Ryan Saenger [a], Irine Neba Mforsoh [b], Arun Shukla [b]

[a] Naval Undersea Warfare Center (Division Newport), 1176 Howell St, Newport, RI, 02841, USA
[b] Dynamic Photo Mechanics Laboratory, Department of Mechanical, Industrial and Systems Engineering, University of Rhode Island, Kingston, RI, 02881, USA

ARTICLE INFO

Article history:
Received 2 April 2020
Received in revised form
12 May 2020
Accepted 13 May 2020
Available online 22 May 2020

Keywords:
Composite material
Low temperature
Mechanical characterization
Water absorption
Fracture

ABSTRACT

An experimental investigation through which the effects of low temperatures on the mechanical, fracture, impact, and dynamic properties of carbon- and E-glass-epoxy composite materials has been conducted. The objective of the study is to quantify the influence of temperatures from 20 °C down to −2 °C on the in-plane (tensile/compressive) and shear material properties, static and dynamic Mode-I fracture characteristics, impact/residual strength, and the storage and loss moduli for the materials considered. The low end of the temperature range considered in the study is associated with Arctic seawater as well as conditions found at extreme ocean depths (2 °C–4 °C). In the investigation, both carbon/epoxy and E-glass/epoxy laminates are evaluated as these materials are of keen interest to the marine and undersea vehicle community. The mechanical characterization of the laminates consists of controlled tension, compression, and short beam shear testing. The Mode-I fracture performance is quantified under both quasi-static and highly dynamic loading rates with additional flexure after impact strength characterization conducted through the use of a drop tower facility. Finally, dynamic mechanical analysis (DMA) testing has been completed on each material to measure the storage and loss moduli of the carbon fiber- and E-glass fiber reinforced composites. The findings of the study show that nearly all characteristics of the mechanical performance of the laminates are both material and temperature dependent.

1. Introduction

A key advantage to the use of fibrous composites in structural design is the ability to customize material performance to prescribed design requirements and operating environments. Fiber-reinforced polymer (FRP) composites provide many readily recognized performance benefits; lightweight, high strength- and stiffness-to-weight ratios, corrosion resistance, net shape manufacturing, and more. Proper selections of the fabric architectures, fiber and matrix materials, ply stacking arrangements, etc. can yield significant mechanical performance advantages over traditional structural materials. Owing to the significant mechanical performance advantages that can be achieved beyond traditional homogeneous and isotropic materials, the marine industries utilize FRP composites in various surface and sub-surface applications. Composite material selections are often made based upon empirical data derived from material level tests, prototype experiments, and/or analytical/computational mechanics models for the required operating conditions. However, when operating environments and loading conditions of systems change beyond their original intended use, reevaluation is generally required to ensure continued functionality and structural integrity. Consideration is made that subsea systems in use in applications such as deep-sea mining or Arctic drilling may not have been originally designed for operations in such low temperature environments. Furthermore, with a consideration of the complexities of composite materials, the community has a limited understanding of failure and fracture mechanisms of FRP composites operating in cold temperature environments. Compared to traditional materials such

* Corresponding author.
E-mail address: James.M.LeBLanc@Navy.Mil (J. LeBlanc).
Peer review under responsibility of Editorial Board of International Journal of Lightweight Materials and Manufacture.

https://doi.org/10.1016/j.ijlmm.2020.05.002

as metals, there is generally a limited understanding of the mechanical and failure/fracture mechanisms of complex composite structures operating in cold environments. Understanding these environmental influences is critical towards the: (1) improvement of fiber and matrix material performance, (2) development of damage and fracture resistant laminate designs, and (3) progress in new manufacturing processes necessary to meet the challenges of operation in cold environments.

Many polymers exhibit increased stiffness and decreased toughness with colder temperatures. Therefore, the potential for unanticipated failure mechanisms to occur with environmentally-dependent material properties is problematic for polymer composites at extreme temperatures. These factors can reduce structural integrity and lead to premature and catastrophic structural failures in low temperature settings. Therefore, material considerations in the design of composite structures subject to cold operating environments require an in-depth understanding of the relationships between laminate stress distributions, ply interface mechanics, hygrothermal behaviors, damage mechanisms, and fracture mechanics. Improving fracture toughness of FRP composites is of greater importance when loading events including impact, wave slap, and implosion may occur in cold environments. Characterizing the effects of cold temperatures on static and dynamic fracture toughnesses using analytical work and controlled laboratory results aids in sensible decision making when considering material selection. Comprehensive knowledge of the effects of temperature on the failure response of FRP composites beyond what is currently known will greatly advance the ability to design and implement future marine based systems.

Variations between fiber and matrix thermal expansions resulting from elevated curing temperature transitioning to ambient temperatures followed by cold operating temperatures can produce damaging residual interlaminar shear stresses and microcracking – even in the absence of applied external loads. Thermally-induced debonding of the fiber-matrix occurs when the interlaminar shear stresses exceed the shear strength of the matrix causing the formation of microcracks. Repeated cold temperature cycles can lead to coalescence of microcracks to the extent that larger interlaminar and intralaminar cracks develop and degrade laminate strength and stiffness levels.

Studies of temperature effects on FRP composites have been limited [1]. Kichhannagari [2] observed from experiments that micro-cracking was more pronounced at cold versus ambient temperatures when specimens were tested under nominal uniaxial and biaxial loads. Thermal contraction causes matrix shrinkage and forms residual interlaminar shear stresses. These stresses degrade the interlaminar shear strength, fatigue life, and laminate stiffness. Microcracks can lead to increased permeability, creating paths for hygrothermal effects [3–5] such as moisture and fluid absorption and swelling at cold temperatures. Swelling is a major source of environmentally-induced stress when laminates are subjected to a freeze-thaw cycling in the presence of water. The generation of microcracks can lead to coalescence which can cause larger mesoscale and macro-scale cracks leading to reductions in fracture toughness and damage tolerance. The effects of freeze-thaw cycles when combined with loading cycles are of significant importance and must be addressed in the design of low temperature structures. Improving fracture toughness of FRP composites is of greater importance when dynamic and impact loading events occurring in cold ocean environments are a concern. Controlled laboratory experiments such as drop tower testing can be performed to simulate these events by which the effects of cold temperatures on static and dynamic fracture toughness can be characterized for optimizing material selections in design. Lopresto et al. [6] investigated the effects of extreme low temperatures, as well as the underlying support conditions, on the compression after impact behavior of composite laminates and identified the effects of water backing during impact. The same authors have also presented findings of the effect of extreme low temperatures on the impact behavior of basalt laminates, including damage onset conditions and energy absorption by the laminates [7].

2. Materials

The materials studied in the investigation consisted of carbon/epoxy and E-glass/epoxy laminates. In each laminate the base fabric was a “plain weave” style in which the yarns are woven in a one-over one-under pattern as shown in Fig. 1. This resulted in a balanced fabric in the warp and weft directions. The E-glass fabric had an areal weight density of 190 g/m^2 (5.61 oz/yd^2), yarn count of 18 in the warp and fill directions, and was in a greige (untreated) condition. The carbon fabric was designated as S 611 which had an areal weight density of 199 g/m^2 (5.88 oz/yd^2), yarn counts of 12.5 in each direction, and was also in the greige condition. The panels were manufactured in a press to maintain uniform thickness and utilized ProSet 125/226 laminating epoxy. They were cured in the press at 82 °C (180 °F), under 14 tons of pressure. To support the various testing requirements, panels of thicknesses of 2.54 and 5.08 mm (0.1 and 0.2 in.) were manufactured.

3. Experimental approach

3.1. Tension/compression/short beam shear

Material characterization in the form of Tension, Compression, and Short Beam Shear was conducted on the carbon and E-glass laminates to determine the effect of decreasing temperature on the stiffness and strength properties. Mechanical testing was conducted in accordance with ASTM D638 (Tension) [9], ASTM D3410 (Compression) [10], and ASTM D2344 (Short Beam) [11], respectively. Each material was characterized for both stiffness and strength at temperatures of 20 °C, 5 °C, and −2 °C. The tests were performed on an Instron® machine operated in displacement-controlled loading, with the low-temperature conditions achieved in an environmental chamber utilizing liquid nitrogen as the cooling source. Prior to the conduct of all tests the specimens were placed in the environmental chamber at temperature for a minimum of 2 h to ensure uniform temperature through the specimen. This was deemed sufficient due to the relative thinness of the specimens. Fig. 2 provides the details of the respective experimental test arrangements.

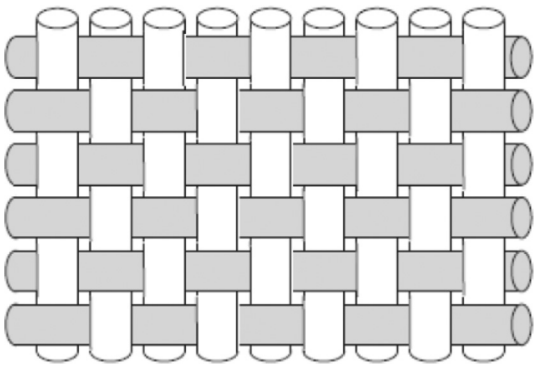

Fig. 1. Plain weave fabric architecture (courtesy of JPS composites technical reference handbook [8]).

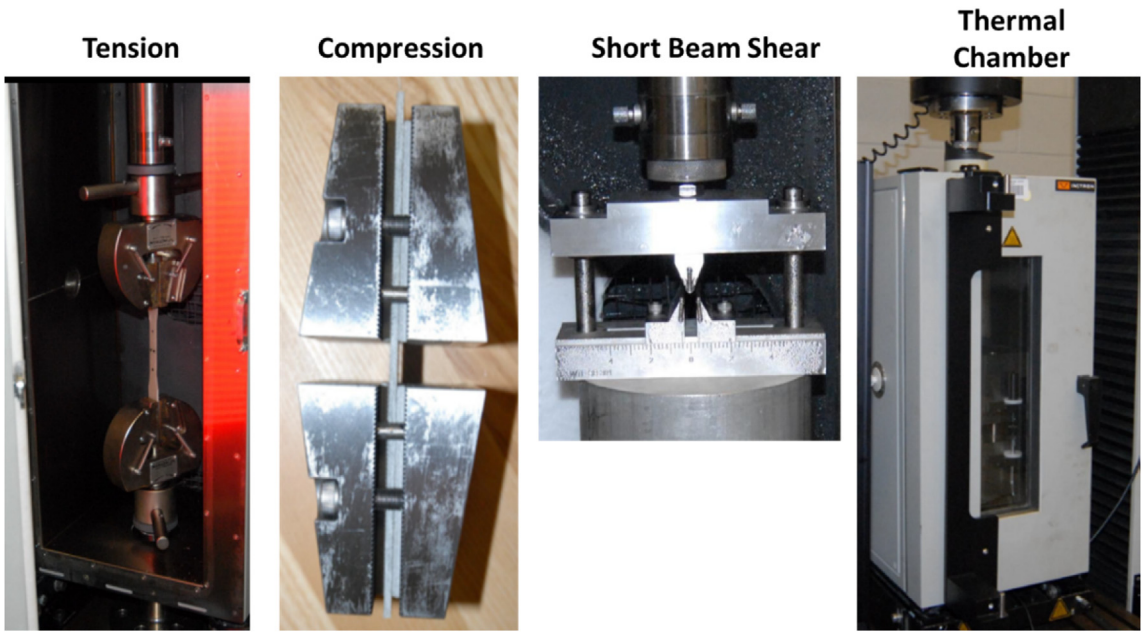

Fig. 2. Tensile, compressive, and short beam shear test setups.

3.2. Static Mode I fracture

Static Mode-I fracture tests were conducted to measure the temperature dependence on the critical strain energy release rates G_{IC} for the carbon and E-glass laminates. The Mode-I fracture tests were performed at 20 °C, 5 °C, and −2 °C to ensure consistency with the mechanical characterization. Specimens were double cantilever beam (DCB) type and fracture gages were bonded to the specimen edges to measure the crack lengths, crack growth stability, and allow calculation of G_{IC}. DCB specimens were 22.80 cm long by 2.54 cm wide (9 in. by 1 in.) and included a 7.62 cm (3 in.) Teflon insert positioned at the mid-plane to serve as a precrack. Single crack gages consisting of 20 strands oriented perpendicularly to the crack front with a strand spacing of 2 mm (0.08 in.) were bonded to one side of each specimen. As the crack front propagated across each strand, the strands broke consecutively and the change in gage resistance was recorded by the data acquisition system. Additionally, the load and deflection time histories were recorded by the test machine. Using the time history data, crack growth and G_{IC} values were characterized.

Upon loading, strain energy is produced in the specimen and a critical load P_c is reached. At this load, the corresponding strain energy causes crack initiation to occur at the end of the Teflon insert. As the deflection of each beam increases further, increases in crack length occur, strain energy is released (lost) and compliance is increased. The load versus deflection curve for the −2 °C E-glass fracture test is shown in Fig. 3 and was representative of the DCB Mode-I fracture test specimen behavior of all samples tested. Strain energy released through Mode-I fracture was calculated by continually monitoring the loads and deflections for each crack length prior to the next increment of crack growth. The method of calculating G_{IC} in the current study is the Modified Beam Theory (MBT) approach. The governing MBT equation is given as [13]:

$$G_{IC} = \frac{3P\delta}{2wa}$$

where P is the load, δ is the extension, w is the specimen width, and a is the crack length.

3.3. Dynamic Mode I fracture

The dynamic fracture characteristics of the carbon and E-glass laminates were obtained using an advanced experimental approach [14]. Dynamic fracture toughness was determined using the wedge-insert-fracture method, which utilized a double

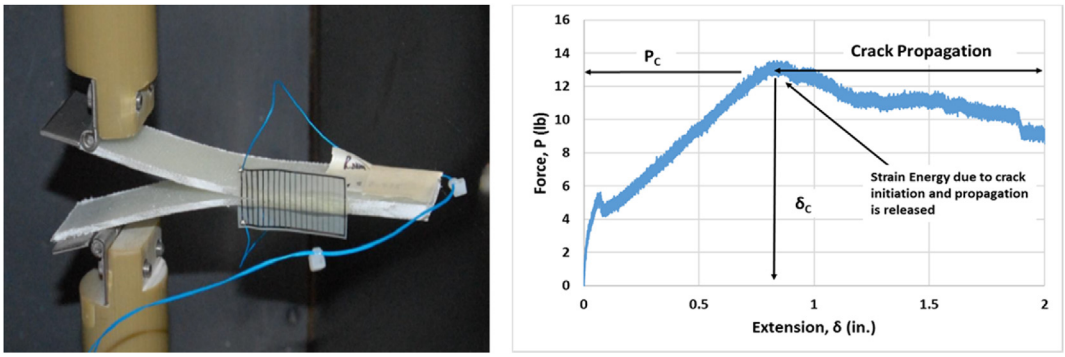

Fig. 3. Mode-I fracture test configuration and typical load vs. extension behavior.

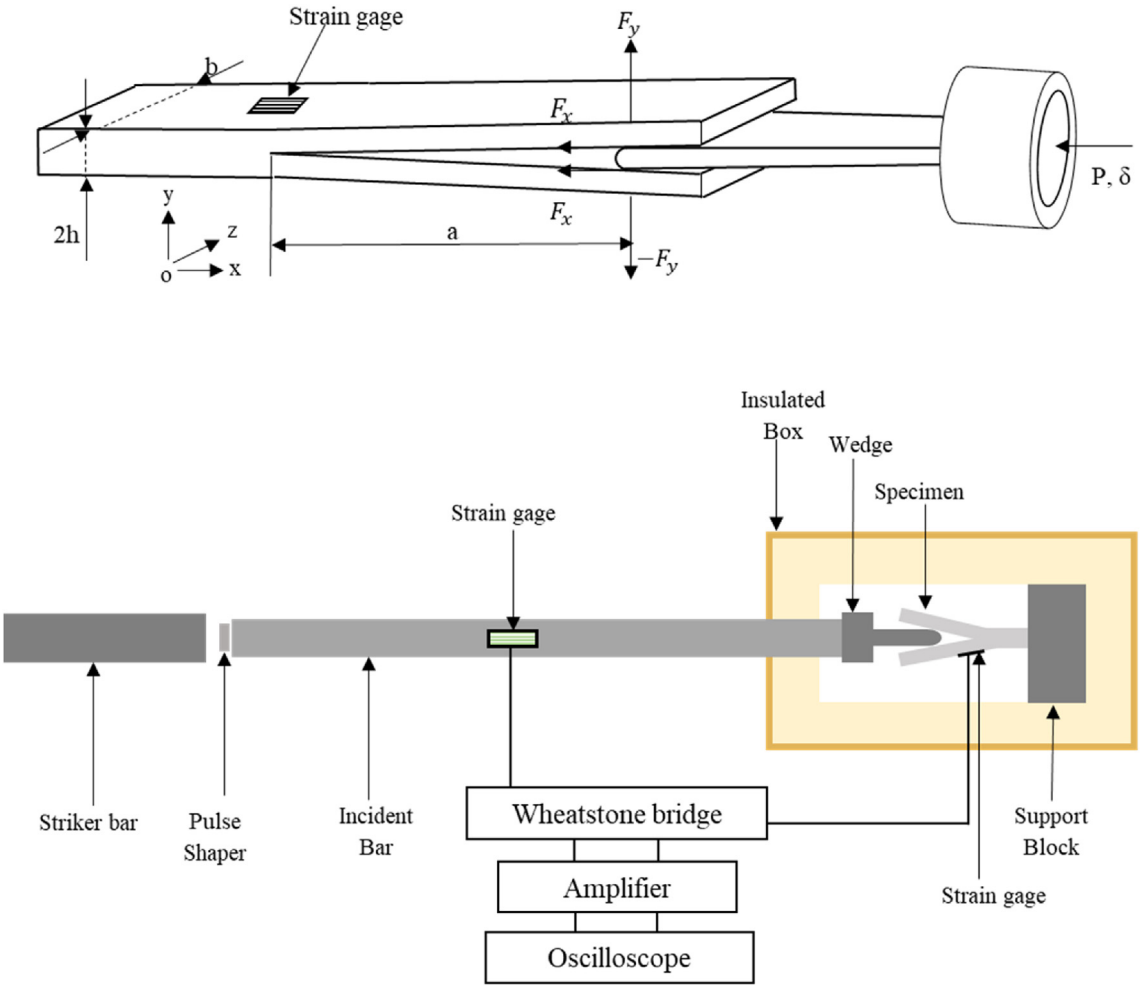

Fig. 4. Dynamic Mode-I fracture setup using Split Hopkinson Pressure Bar.

cantilever beam specimen geometry combined with a unique Split Hopkinson Pressure Bar (SHPB) setup shown in Fig. 4. The specimen had a width of 12.70 mm (0.5 in.) and a thickness of 5.08 mm (0.2 in.) with a Teflon film insert used as a precrack at the mid plane of the panel. The incident bar was 9.5 mm (0.375 in.) in diameter, 162 cm (64 in.) in length and was made out of brass. The portion of the wedge insert in contact with the incident bar had a 12.7 mm (0.5 in.) outer diameter and the flat end in contact with the specimens was semi-cylindrical with a diameter of 3 mm (0.118 in.). The initial crack length (distance from the center of the semi-cylindrical tip of the inserted wedge to the crack tip), was 4.7 cm (1.85 in.) and 4.2 cm (1.65 in.) for the carbon/epoxy composite and E-glass/epoxy composite, respectively.

During each experiment, the striker bar driven by a gas gun impacted the incident bar creating a compressive pulse in the bar which was measured using two resistive strain gages bonded on the incident bar, opposite to each other. At the point of contact, the impact force is resolved into two components, F_x and F_y, as seen in Fig. 4. A strain gage was bonded to the upper surface of the specimen with its center at the point $(x, y) = (0, h)$. This strain gage measured the surface strains which were used for the estimation of the vertical component of the impact force, F_y and subsequently for the calculation of the dynamic critical energy release rate, G_{ICd}. The component of the energy release rate related to the horizontal component of the force, F_x was neglected because the radius of wedge tip was very small compared to the initial crack length. During the experiment, the end of the specimen without a crack rested on a support block and the crack opening was ensured to be symmetrical. The experiments conducted at 5 °C and −2 °C utilized a wooden cooling box with glass fiber insulation as shown in Fig. 5. Compressed air circulated in a copper tube, immersed in dry ice, was used to cool the specimen in the cooling box. The desired specimen temperatures were achieved by controlling the flow rate of the compressed air with real-time measurements of the temperature in the box recorded using a K-type thermocouple. Upon the specimen reaching thermal equilibrium with the air in the cooling chamber, the striker was released to create the compressive pulse in the incident bar. Clay was used as a pulse shaper on the striker end of the incident bar to eliminate the high frequency components of the compressive pulse, thus effectively suppressing vibrations on the specimens caused by impact loading.

The dynamic energy release rate for the Mode-I Dynamic DCB specimen is given by:

$$G_{Id} = \frac{F_y^2}{2b}\frac{\partial C}{\partial a} \tag{1}$$

where F_y is the vertical component of the force, b is the width of the specimens, a is the initial crack length and C is the compliance of the specimen.

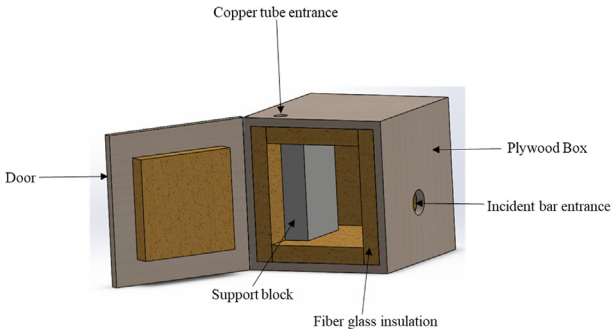

Fig. 5. SHPB cooling box schematic.

The specimen compliance is given by

$$C = \frac{\delta}{F_y} = \frac{a^n}{H} \tag{2}$$

where $n = 3$ and $H = \frac{3}{2}E_{xx}I$. E_{xx} is the Young modulus in the longitudinal direction and I is the moment of inertia of each beam of the specimen given by $I = \frac{bh^3}{12}$.

Substituting equation (2) in equation (1) and simplifying gives the dynamic energy release rate as:

$$G_{Id} = \frac{{F_y}^2 a^2}{bE_{xx}I} \tag{3}$$

For the effective crack length $n(a)$, a correction factor for local deformation around the crack tip, e is included. Due to the orthotropic nature of the material the value of e is high and cannot be neglected; e was considered to be 3 mm (0.118 in.) in these experiments and the final form of the energy release rate is

$$G_{Id} = \frac{{F_y}^2 (a+e)^2}{bE_{xx}I} \tag{4}$$

The SHPB is used to apply the force longitudinally through the wedge. The force can be calculated from the surface strains at the crack tip. These strains are measured using a strain gage of very small gage length to minimize averaging effects in the longitudinal direction and obtain localized values. Utilizing beam theory, the surface strain at any point on the surface of the specimen is given by:

$$\varepsilon_x = \frac{\sigma_x}{E_{xx}} = \frac{M(h/2)}{E_{xx}I} \tag{5}$$

where σ_x, is the stress on the beam and M is the moment. Also, the strains from the strain gage are given by equation (6).

$$\varepsilon_s = \frac{\Delta l}{l} = \int_{e-l/2}^{e+l/2} \frac{\varepsilon_x dx}{l} \tag{6}$$

where l is the gage length. Solving equation (6) results in an expression for the force in the case of dynamic loading.

$$F_y = \frac{2\varepsilon_s E_{xx} I}{ha} \tag{7}$$

Substituting equation (7) in (4) yields G_{Id} for the Wedge-Insert-Fracture (WIF) specimen

$$G_{Id} = \frac{h{\varepsilon_s}^2 E_{xx}(a+e)^2}{3a^2} \tag{8}$$

The Mode-I critical strain energy release rate is calculated from equation (8), using the maximum value of strains attained. In these experiments and in lieu of using the strain rate, the loading rate was calculated as the time derivative of the energy release rate.

3.4. Impact and Flexure after impact

The dependence of impact loading performance as a function of temperature for each composite material was evaluated through a sequential test series involving a drop tower impact test followed by 4-point flexure after impact tests. The methodology is consistent with that utilized in Ref. [12] for generating barely visible impact damage (BVID) levels and is summarized briefly here for completeness.

The impact experiments were performed on an Instron Dynatup® Model 9210 drop test machine with rectangular specimens of geometry 139.7 mm × 12.7 mm × 0.508 mm (5.5″ × 0.5″ × 0.2″). The warp direction of the material corresponds to the length direction of all impact specimens. The line-load impactor was 6.35 mm (0.25″) in radius and was instrumented with an accelerometer to record the impact force time history for each event. The arrangement for the impact experiments consisted of a three-point flexure configuration with a span length between supports of 5.08 cm (2″) as shown in Fig. 6. The primary intent of the impact testing was to: (1) obtain the force-time history of each impact test, and (2) impart an observable level of damage to the specimens for the subsequent four-point flexural after impact testing. Prior to the conduct of each impact test, the specimens were “Thermally Soaked” for a minimum of one hour in a separate thermal chamber to achieve the desired specimen temperature and then immediately placed in the drop tower and the test conducted. After each test the specimens were returned to the thermal chamber to ensure consistent temperatures with the subsequent flexural tests. In order to determine suitable levels of impact energy that result in damage but not complete failure of the specimens, initial trial runs were conducted at various energy levels to establish an acceptable energy threshold (AET) for producing damage commensurate with visible impact damage levels. The impact energy was determined for the room temperature specimens and used for the low temperature tests. The respective impact energies used in the study were 5.3J for the carbon laminates and 8.6J for the E-glass laminates. The post-impact material damage levels for the drop test conducted at 5 °C for the carbon and E-glass laminates are shown in Fig. 7.

Subsequent to the drop tower impact tests, four-point flexural bending tests were conducted with the primary intention to quantify the effect of temperature on residual flexure strength after impact of

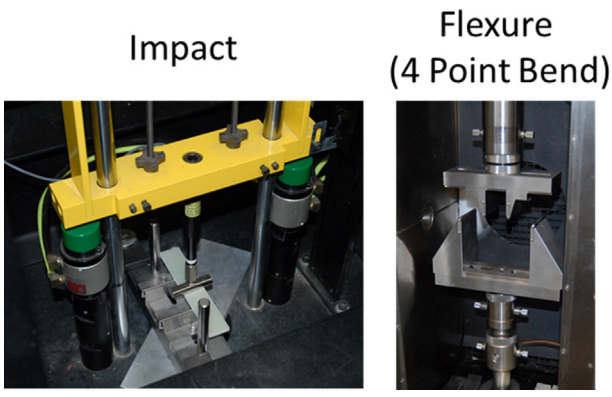

Fig. 6. Drop tower impact and flexure after impact test setups.

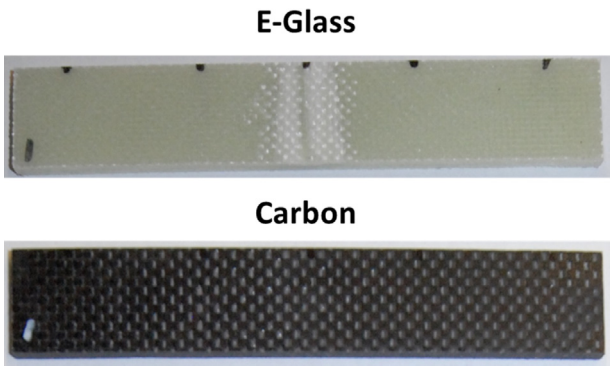

Fig. 7. 5 °C impact test damage levels.

the respective laminates. In a consistent manner with the tensile and compression testing previously discussed, the four-point flexure loading was performed on the Instron test machine with a low temperature environmental chamber installed to ensure consistent temperature for the duration of the tests. A four-point flexure-loading fixture with cylindrical steel rollers as shown in Fig. 6 was used for the characterization. The overall span length for the tests was 114.3 mm and the span between loading supports was 38.1 mm.

3.5. DMA

The storage and loss moduli of the carbon and E-glass laminates were characterized through the use of Dynamic Mechanical Analysis (DMA). Dynamic mechanical analysis is based on the application of small-amplitude, time-oscillatory mechanical forcing to a material sample and the simultaneous measurement of displacement, force magnitude and phase. In this study, the perturbations are applied by a displacement-controlled drive shaft that bends the specimen. Although the materials in this study are not isotropic, normal strain parallel to the specimen's neutral axis is the dominant deformation mode in beam bending. The specimens were small beams 5.6 mm (0.22 in.) wide and 35.5 mm (1.4 in.) long and a TA Q800 DMA machine with a 20 mm dual-cantilever clamp was utilized as shown in Fig. 8. The composite sample beams were excited by time-oscillatory loads between 1 and 100 Hz at temperatures from −100 °C to 180 °C, a range that includes the glass transition temperature, T_g. A time-temperature superposition technique enabled estimation of the high-frequency storage and loss moduli of the composite specimens. All mechanical properties measured by DMA in this study are measured in the weft direction. The tangent of the phase between stress and strain is a measure of the ratio of the loss modulus of the material to its storage counterpart, $\tan\delta = \mathrm{Im}(\tilde{E})/\mathrm{Re}(\tilde{E})$ [15].

A number of specimens were preliminarily characterized by loading them in tension (x-direction) in order to measure the small strain as a function of stress at a number of frequencies (1 Hz, 10.8 Hz, 100 Hz, and 200 Hz). At all strain rates and strain levels under 0.075% the composites exhibited an elastic modulus of 4.9 GPa and 9.17 GPa for the E-glass and carbon composite, respectively. Fig. 9 shows that the linear viscoelastic behavior at small strains is a matrix dominated behavior with a composite (fiber and matrix combined) behavior emerging at higher strain rates at strain levels greater than 0.075%. The carbon laminates exhibit this behavior transition at a lower strain level than that seen in the E-glass laminates. Note the increasingly dissipative nature of the carbon laminates at strain levels approaching 0.1% at a root mean-squared (RMS) strain rate of 0.7 rad/s. Therefore, at this level of strain and strain rates the carbon laminate's stress state is history-dependent.

4. Experimental results

4.1. Mechanical characterization

The tensile and compressive mechanical characterization results for the carbon and E-glass tests conducted at 20 °C, 5 °C, and −2 °C are shown in Fig. 10 and summarized in Table 1 and Table 2. In all cases, the individual tests showed that material response is nearly linear up to failure and the failure was classified as brittle in nature such that there was minimal plastic response as shown in Fig. 11. From the presented results there are evident trends in material response over the temperature range considered in the study. The experimental results show that in terms of stiffness performance, both the carbon and E-glass laminates are significantly stiffer in tension that compression. For the carbon laminates there is a difference of nearly an order of magnitude and for the E-glass laminates the compressive stiffness is 25% of that of the tensile.

The tensile results showed that the carbon laminates were about five times stiffer on average than the E-glass laminates across all temperatures, 58.6 GPa vs. 11.3 GPa (8500 ksi vs. 1645 ksi), and had slightly more than double the strength of the E-glass laminates. Furthermore, the E-glass laminates did not demonstrate a significant dependence on decreasing temperature across the range considered. It should be noted that the mechanical results presented considered in this section are laminate representative properties (fiber and matrix contributions) versus DMA

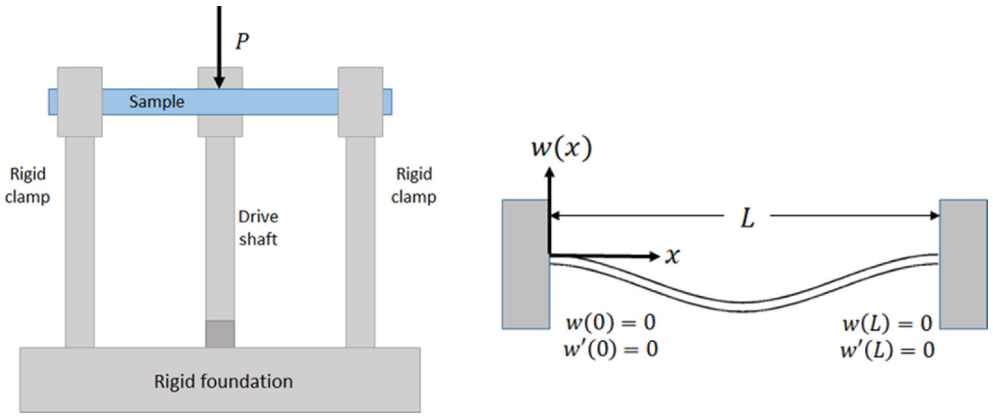

Fig. 8. Dual-cantilever clamp and deflection boundary conditions.

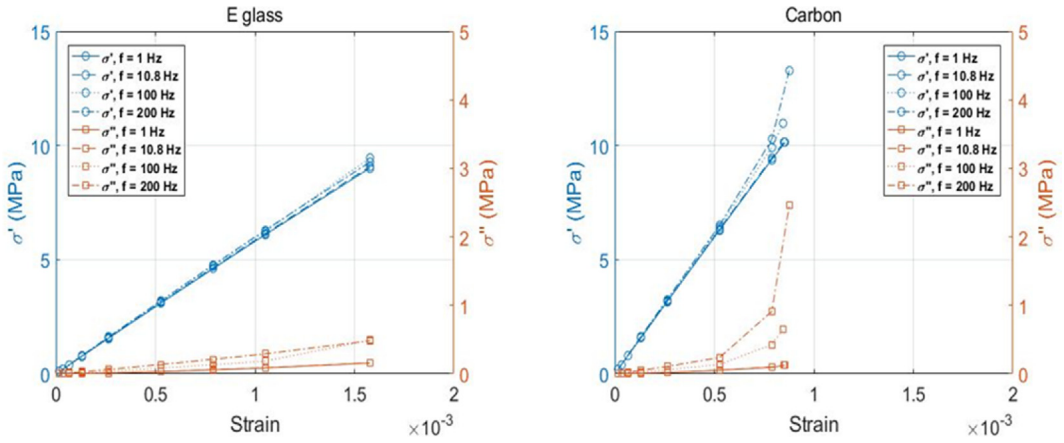

Fig. 9. Stress-strain behavior of E-glass and carbon laminates showing both elastic (left axes) and viscous (right axes) stresses.

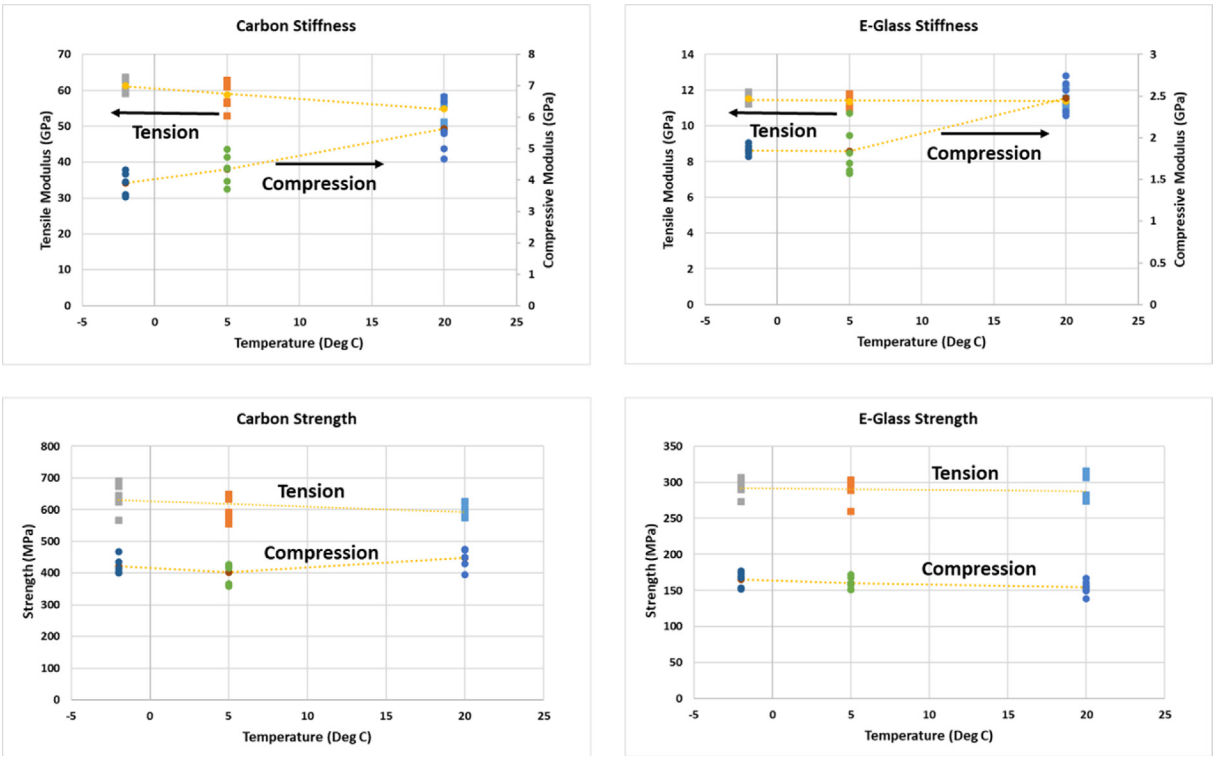

Fig. 10. Tensile and compressive mechanical characterization.

Table 1
E-Glass mechanical property summary.

	E-Glass		
	20 °C	5 °C	−2 °C
Tensile Modulus (GPa)	11.39 ± 0.40	11.34 ± 0.26	11.51 ± 0.20
Compressive Modulus (GPa)	2.47 ± 0.18	1.83 ± 0.25	1.84 ± 0.06
Tensile Strength (MPa)	288.31 ± 16.18	288.08 ± 13.38	293.48 ± 10.86
Compressive Strength (MPa)	154.21 ± 9.07	160.06 ± 7.76	165.49 ± 9.39
Short Beam Shear Strength (MPa)	27.73 ± 1.36	33.26 ± 0.87	33.76 ± 0.76

results, which are presented later, are primarily representative of the matrix material. Both the tensile modulus and tensile strength were statistically equal at each temperature ranging from 20 °C to −2 °C. Conversely, The carbon laminates exhibit a dependence on the test temperature in that under tension these laminates became both stiffer and stronger as the temperature decreased from 20 °C to −2 °C. The modulus displayed an 11% increase and the strength displayed a 7% increase over the temperature range,

Table 2
Carbon mechanical property summary.

	Carbon		
	20 °C	5 °C	−2 °C
Tensile Modulus (GPa)	54.82 ± 3.32	58.74 ± 3.65	61.30 ± 1.84
Compressive Modulus (GPa)	5.64 ± 0.72	4.35 ± 0.42	3.89 ± 0.34
Tensile Strength (MPa)	595.70 ± 16.01	607.77 ± 35.19	637.53 ± 39.36
Compressive Strength (MPa)	448.98 ± 29.02	401.80 ± 28.05	420.72 ± 23.96
Short Beam Shear Strength (MPa)	52.87 ± 0.59	62.64 ± 0.95	66.18 ± 0.64

hence an inverse relationship between tensile performance and temperature.

In compression, there are several trends that were identified. Specific to the compressive behavior, the carbon laminates were approximately two times stiffer than the E-glass laminates across all temperatures. The carbon laminates had approximately 2.5 times the compressive strength of the E-glass laminates across the temperature range. The specific E-glass/epoxy laminates utilized in this study exhibited differing trends in moduli and strength with decreasing temperature. As evidenced from Fig. 10, it was seen that with decreasing temperature there was a decrease in compressive modulus but a corresponding increase in compressive strength. In other words, as the temperature was reduced, the material became softer but stronger. The carbon/epoxy laminates exhibited a clear trend with decreasing temperature, a decrease of 30% over the range from 20 °C to −2 °C. Similarly, the material strength exhibited a decrease from 20 °C to 5 °C, but then remained statistically constant from 5 °C to −2 °C.

The short beam shear strength characterization trends of the carbon and E-glass are presented graphically in Fig. 12 for both overall stress-displacement history and temperature trends and summarized in Tables 1 and 2. The displacement time history is presented for the −2 °C for brevity but similar trends are seen for all temperatures considered. From these results there were several trends that can be observed as follows. In terms of overall short beam shear strength, the carbon laminates exhibited approximately twice the strength as compared to the E-glass laminates at a given temperature. The E-glass/epoxy laminates were characterized by a flat plateau in stress with increasing displacement after reaching maximum load whereas the carbon laminates exhibited decreasing stress capacity after maximum load. The carbon and E-glass laminates exhibited a 20% increase in short beam shear strength over the range from 20 °C to −2 °C.

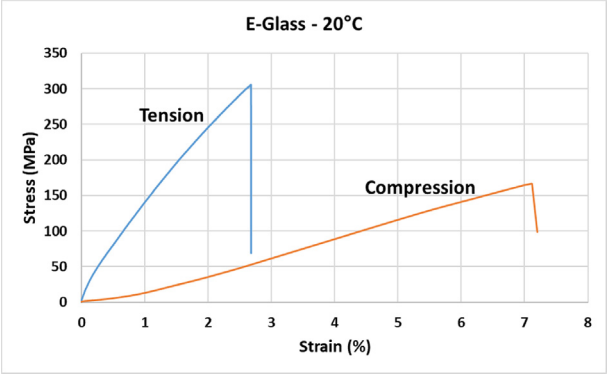

Fig. 11. E-glass tensile and compression representative behavior (20 °C).

4.2. Static Mode-I fracture

The Mode-I fracture characteristics of the carbon and E-glass laminates are quantified through the calculation of G_{IC} using the method previously discussed. The strain energy release rate, G_{IC}, for each laminate is provided in Fig. 13 with a corresponding summary of the results in Table 3. From the respective figures, it is seen that each laminate material exhibits a direct dependence of G_{IC} on temperature, namely that with decreasing temperature there is a corresponding decrease in G_{IC}. For the E-glass laminate the G_{IC} value (1400 J/m^2) at −2 °C is 65% of the corresponding value at 20 °C (2100 J/m^2). The Carbon laminates exhibit less dependence on temperature than the E-glass laminates. There is a very small decrease in G_{IC} from 20 °C to 5 °C, and a statistically constant value from 5 °C to −2 °C. The differing trends in fracture behavior between the carbon and E-glass laminates indicates that the strain energy release rate, G_{IC}, is primarily a function of fiber material and not matrix material for these laminates.

4.3. Dynamic Mode-I fracture

The Mode-I critical strain energy release rate for the carbon and E-glass laminates at each of three temperatures (five specimens per temperature) are shown in Fig. 14 and Table 4. The loading rate, taken to be the rate of change of the strain energy release rate with time, was calculated for the E-glass and carbon laminates to be 174.8 kN-m/m^2-s and 113.6 kN-m/m^2-s (1000 in-lb/in^2-s and 650 in-lb/in^2-s) respectively. As was seen with the static fracture results, several trends are apparent. Firstly, the E-glass laminates exhibit larger values for Mode-I critical strain energy release rates than the carbon laminates. Furthermore, the E-glass laminates exhibit a larger dependence on temperature than the carbon laminates. Of more significance is the overall observation that the dynamic G_{ICd} values are markedly lower than the corresponding static values, approximately 6 times lower for the E-glass laminates and 15 times

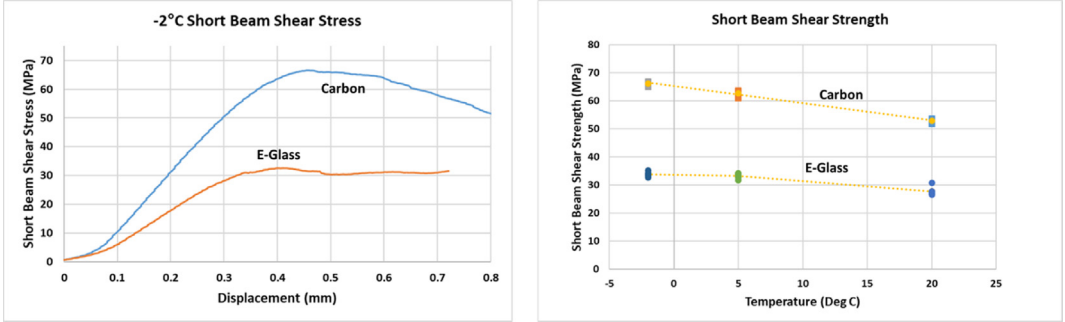

Fig. 12. Short beam shear mechanical characterization.

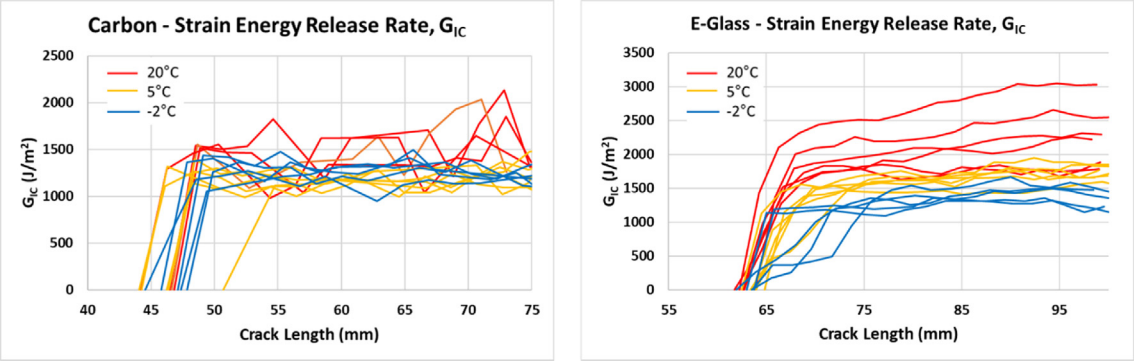

Fig. 13. Strain Energy Release Rate G_{IC} vs. Crack Length.

Table 3
Static Mode-I strain energy release rate summary.

	Static Strain Energy Release Rate, G_{IC} (J/m^2)		
	20 °C	5 °C	−2 °C
Carbon	1462.7 ± 89.02	1181.6 ± 45.82	1245.6 ± 67.70
E-glass	2088.6 ± 348.7	1604.1 ± 75.2	1343.4 ± 104.7

Table 4
Dynamic Mode-I strain energy release rate summary.

	Dynamic Strain Energy Release Rate, G_{IC} (J/m^2)		
	20 °C	5 °C	−2 °C
Carbon	87.85 ± 14.98	92.05 ± 17.38	62.3 ± 17.34
E-glass	317.1 ± 118.55	281.05 ± 71.63	214.90 ± 58.67

lower for the carbon laminates. After careful observation of the fracture surfaces shown in Fig. 15, it was concluded that interfacial fracture between the fiber surface and the matrix occurred during dynamic experiments instead of matrix failure. This interfacial fracture toughness is much lower than the intrinsic fracture toughness of the matrix material.

4.4. Impact and Flexure after impact

The impact behaviors of the carbon and E-glass laminates as quantified by the force-time histories recorded during the drop tower tests are shown in the upper plots of Fig. 16 and summarized in Table 5 and Table 6. In considering the respective force histories there are multiple observations that are drawn regarding both the material and temperature dependencies. As it relates to the effects of decreasing temperature on the impact response, there is no significant apparent dependency on temperature for the E-glass and carbon materials. For all temperatures the peak recorded force is consistent for a given material across all temperatures considered, as is the overall time duration of the event. The carbon laminates impacted with an energy of 5.3 J exhibit a peak force during impact of 6500 N and an overall impact event time of between 3.5 and 4.5 ms. Exhibiting a similar trend in consistent temperature response, the E-glass laminate results in peak impact forces of 3500 N with a corresponding event duration on the order of 8 ms. What is more apparent in observing the results, are significant differences in behavior when comparing the materials. The carbon, owing to its higher stiffness, yields larger peak impact forces than the corresponding E-glass laminates despite being impacted at a 40% lower energy. Furthermore, in observing the force histories beyond the peak value it is shown that that carbon laminates exhibit brittle damage mechanisms unlike the E-glass. Brittle failures are characterized by the high frequency force-time histories observed for the carbon laminates beyond their peaks as well as the much shorter overall duration of the event. The E-glass laminates demonstrate more controlled and gradual damage mechanisms as evidenced by their smoother force-time histories and gradual (longer duration) arresting of the impactor energy during the impact event itself.

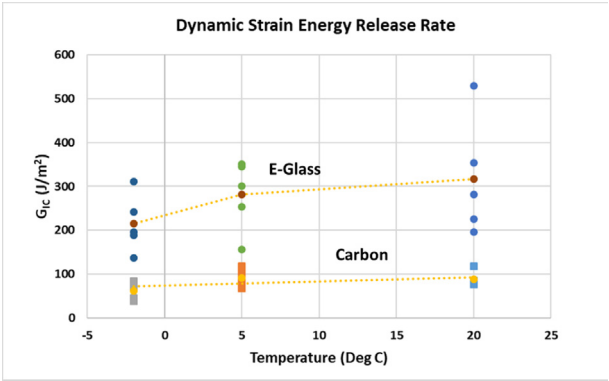

Fig. 14. Dynamic Mode-I critical strain energy release rate, G_{ICd}.

The post-impact four-point flexural behavior of the respective laminates is shown in the lower images of Fig. 16 (Note: Due to the large differences in flexural strength the axis limits have not been adjusted for each material). Observation of the carbon laminate results further support the brittle nature of the material damage. As the material is inherently more brittle and heavily influenced by minor variations in loading and laminate response, there is significant data scatter amongst all temperatures. This is clearly illustrated by the 5 °C samples in which despite all samples being impacted identically, the residual flexural strength ranges from 150 to 400 MPa. This wide range of strength values, even after highly controlled impact experiments, highlights the inherent unknowns and risks when utilizing the carbon laminates for dynamic/impact loading events. Conversely, the E-glass results exhibit tighter groupings of flexural stiffness and strengths within a given temperature band. Overall, there is a readily observable increase in residual flexural strength with decreasing temperature. The specimens impacted at 20 °C have an average residual strength of 120 MPa whereas the samples impacted at −2 °C have an average strength of 170 MPa. Furthermore, The E-glass laminates exhibit flexural strain values between 1.25% and 1.75% whereas the carbon laminates have flexural strain values between 0.75% and 1.1%.

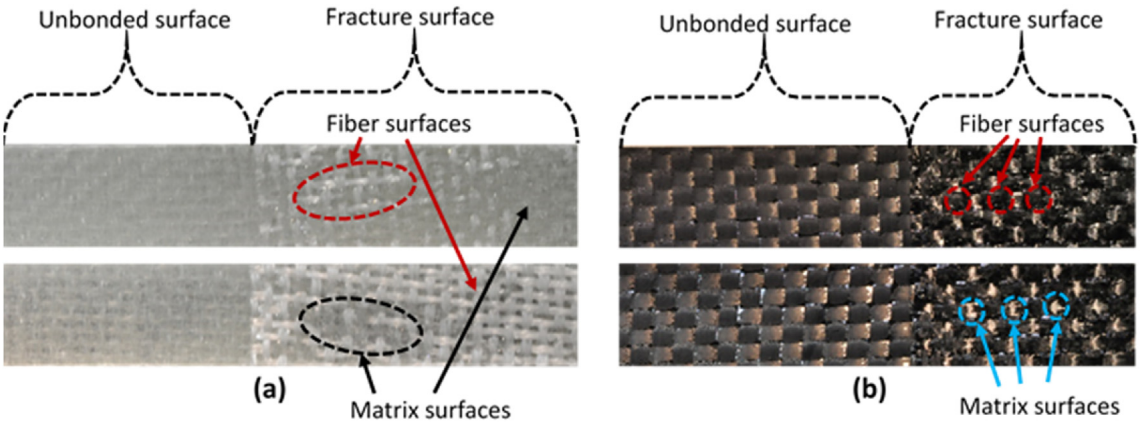

Fig. 15. Dynamic fracture surfaces for (a) E-glass/epoxy and (b) carbon/epoxy composites.

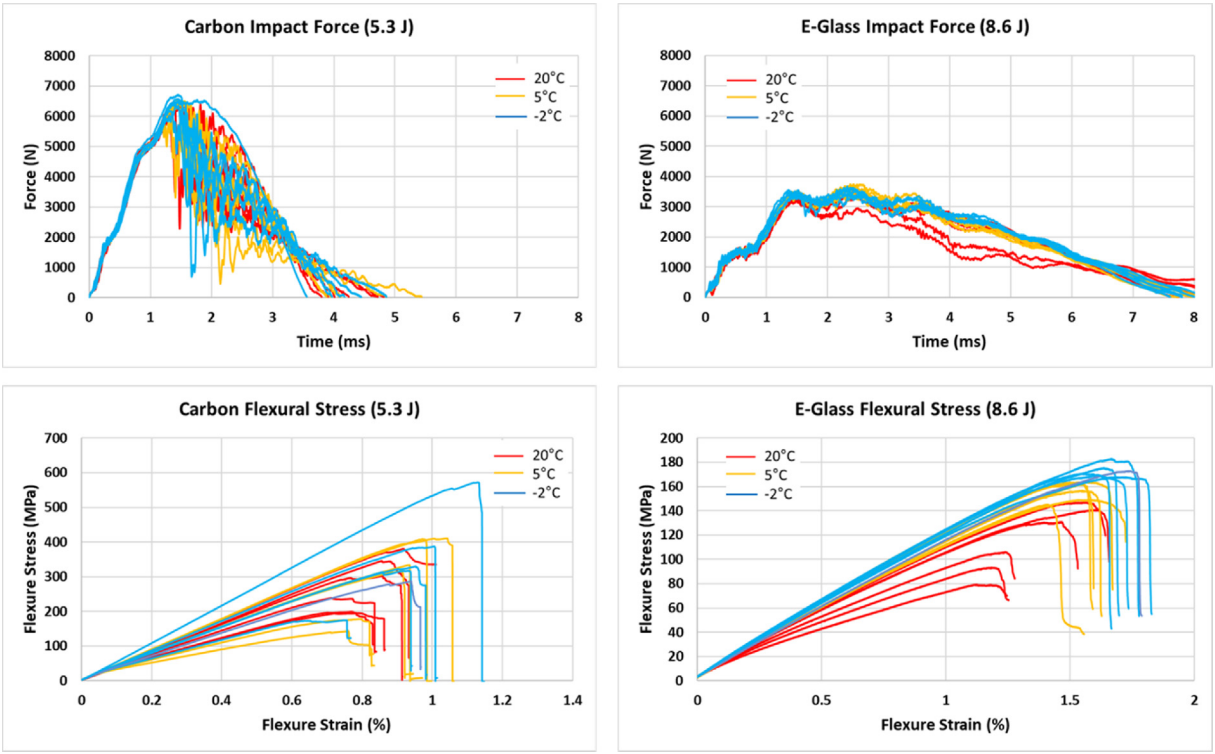

Fig. 16. Impact and flexure after impact performance.

Table 5
Carbon impact and flexure after impact summary.

	Carbon		
	20 °C	5 °C	−2 °C
Maximum Impact Force (N)	6269 ± 157.43	6358 ± 91	6490 ± 145.97
Maximum Flexural Stress (MPa)	277.11 ± 70.81	298.83 ± 103.69	345.02 ± 120.1

Table 6
E-glass impact and flexure after impact summary.

	E-glass		
	20 °C	5 °C	−2 °C
Maximum Impact Force (N)	3401 ± 85.83	3608 ± 110.99	3548 ± 93.50
Maximum Flexural Stress (MPa)	116.23 ± 24.96	156.66 ± 7.28	173.19 ± 5.00

4.5. Dynamic mechanical analysis

The most significant changes in the mechanical properties of polymers take place around T_g where polymer mobility increases and above which entropic elasticity allows molecules to unravel at certain time scales. In order to study the viscoelastic properties of the FRC at a range of frequencies beyond that range which is possible with the dynamic mechanical analyzer (TA Q800 DMA machine), the time-temperature superposition (TTS) technique was used to generate curves that capture the major features of the

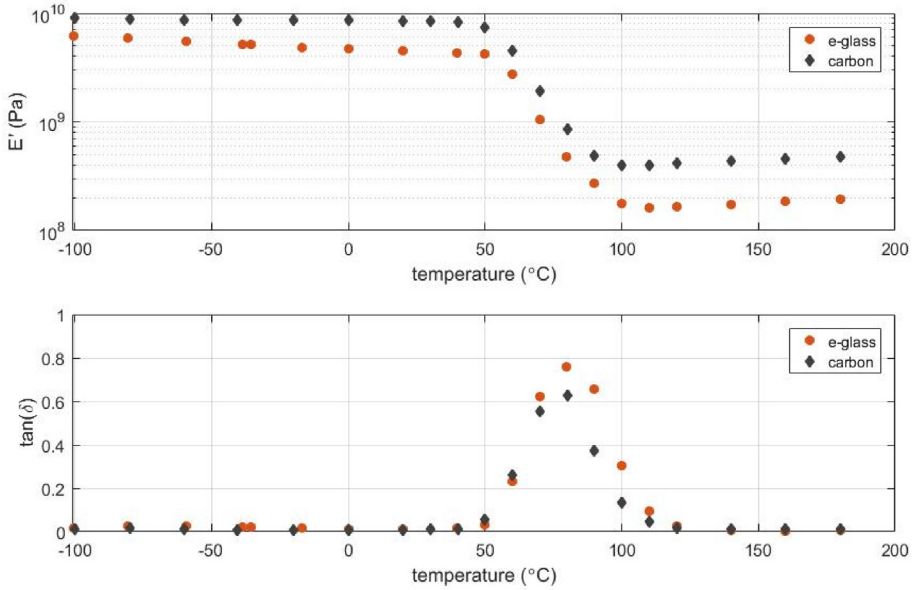

Fig. 17. Fiber reinforced composite storage and loss moduli at 1 Hz.

polymer's dependence on time and temperature. To perform the TTS analysis a beam for each material specimen was installed into the 20 mm dual-cantilever clamp and subsequently enclosed within the DMA's temperature-controlled oven, which was equilibrated initially to −100 °C and held for a period of 3 min. The clamp was then re-tightened around the specimen, to correct for changes in volume due to thermal stresses, before beginning the first frequency sweep. The sample was then held at −100 °C for another 2 min. The sample was perturbed with displacements amplitudes of 12 μm (corresponding to 0.07% maximum strain) during the frequency sweeps. Each frequency sweep consisted of 17 points with logarithmic spacing (8 points per decade) from 1 Hz to 100 Hz. Sweeps were performed at 20 °C intervals from −100 °C to 20 °C, 10 °C intervals from 40 °C to 120 °C, and 20 °C intervals from 140 °C to 180 °C. After equilibrating to the new temperature, the oven executed a 5-min isothermal hold before beginning the frequency sweep. Force, displacement magnitude, and phase angle (δ) were recorded at each frequency point. After the 20 °C equilibration and before the subsequent isothermal hold, the clamp was loosened and re-tightened to prevent thermal expansion from causing high stresses due to clamping. Procedures for DMA of the carbon laminates were similar to those of E-glass, although the ordering of the test frequencies in the sweep was changed from ascending (1–100 Hz) to descending (100–1 Hz).

Temperature dependent behavior of the storage modulus (E') and loss factor ($\tan\delta$) at 1 Hz is shown in Fig. 17. The characteristic

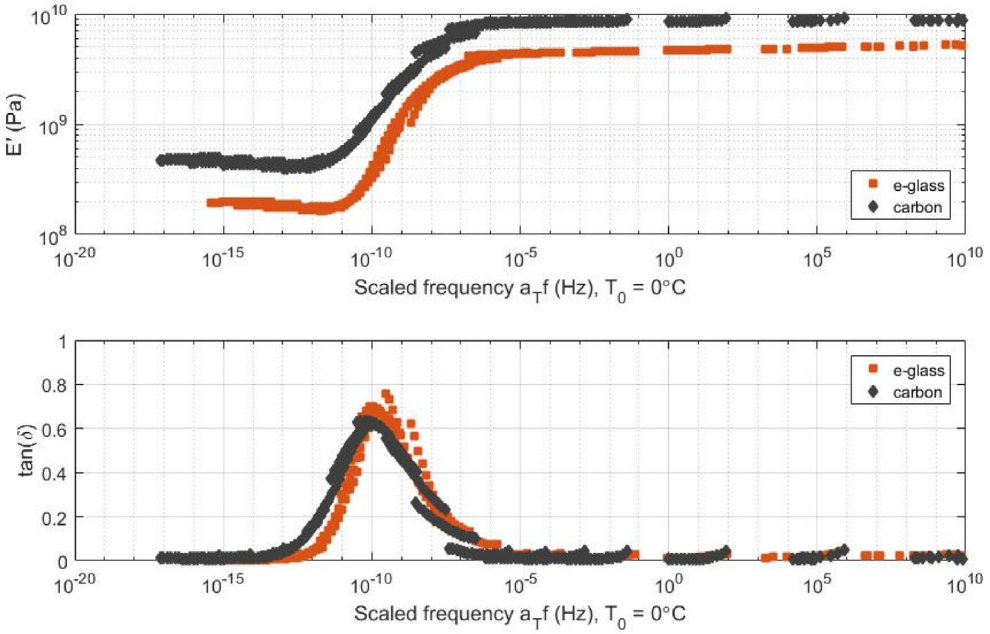

Fig. 18. Storage and loss moduli for E-glass and carbon laminates scaled to 0 °C.

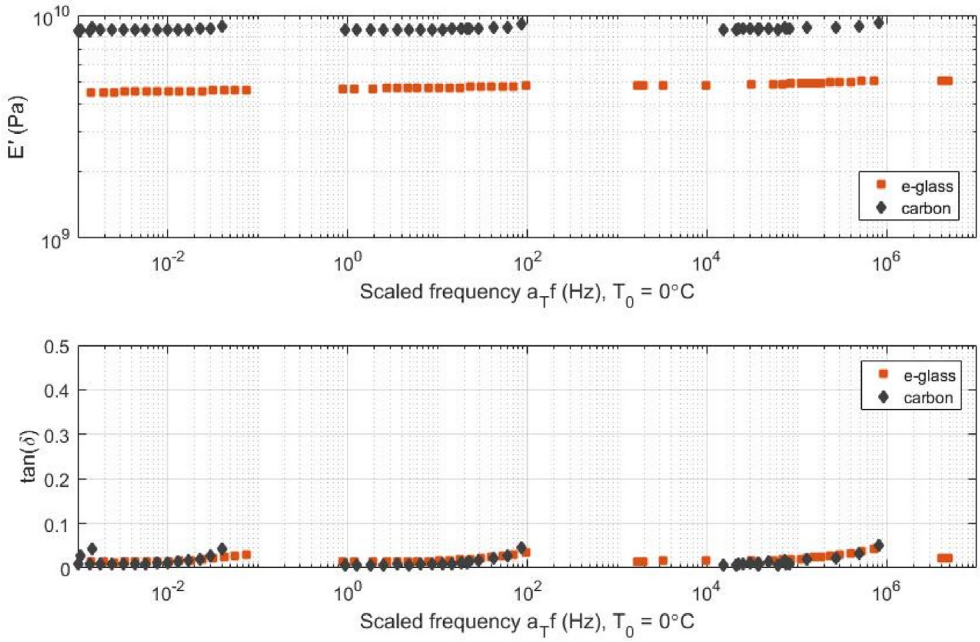

Fig. 19. Storage and loss moduli for E-glass and carbon laminates at relevant frequencies for physical processes.

glass transition behavior was observed, identified by a significant decrease in storage modulus and a corresponding peak in viscoelastic dissipation as the temperature passes through the T_g. Both carbon and E-glass laminate glass transition temperature was measured at the tan δ peak to be approximately 80 °C.

The storage moduli and tan δ from individual frequency sweeps were assembled into master curves by adjusting the parameters C_1 and C_2 of a modified version of the Williams, Landel, and Ferry (WLF) equation and assuming $b_T \approx 1$

$$a_T = \frac{\eta}{\eta_0} = \exp\left(\frac{-C_1(T - T_0)}{C_2 + T - T_\infty}\right) \tag{9}$$

to achieve continuity in scaled frequency $\alpha_T \omega$. The values of C_1 and C_2 that best fit this criterion were approximately 70 and 180 K, respectively for the E-glass laminate. The Carbon laminate was best fit with values of 80 K and 190 K for C_1 and C_2, respectively. T_∞ was 278 K for both laminate types.

Expressing these curves in terms of their corresponding real frequencies, in Hertz and at a temperature of 0 °C, merely requires removal of the scaling term a_T as it evaluates at that temperature. The master curves for the moduli of E-glass and carbon laminates at a reference temperature of 0 °C are shown in Fig. 18. They reveal that there is little reason to expect polymer-related losses in material transmission frequencies at Arctic temperatures since the tan δ values are less than 0.1 above frequencies on the order of 10^{-3} Hz (Fig. 19). The mechanical properties of fiber-reinforced epoxy composites are essentially constant within the frequency ranges of interest in acoustics. This is perhaps unsurprising given the high T_g of most epoxies.

5. Conclusions

A detailed experimental investigation of the effects of low temperature on the mechanical, fracture, and frequency dependent material properties of E-glass/epoxy and carbon/epoxy laminates has been conducted. The investigation was primarily aimed at establishing a foundational understanding of the temperature effects on composite laminates at temperatures of interest to the marine community. Historically, mechanical and acoustic properties at operating temperatures in the range of 15 °C–20 °C have been evaluated, with minimal data pertaining to the temperatures associated with Arctic seawater in the 2 °C–4 °C regime. The key findings of the study were as follows:

5.1. Mechanical performance

(1) Tension: The specific E-glass/epoxy material investigated exhibited a minimal dependence on decreasing temperature in terms of elastic modulus and tensile strength. There is a measurable dependence on decreasing temperature for the carbon/epoxy laminate evaluated with the material both stiffening and strengthening over the range 20 °C to −2 °C. Specifically, an 11% increase in modulus and a 7% increase in strength with decreasing temperature. Hence an inverse relationship between tensile performance and temperature.
(2) Compression: The specific E-glass/epoxy material utilized in this study exhibited opposite trends in stiffness and strength with decreasing temperature. As the temperature is decreased the material became softer but stronger. Carbon/epoxy laminates exhibited decreasing stiffness with decreasing temperature, a decrease of 30% over the range considered, and a material strength decrease from 20 °C to 5 °C followed by near constant strength from 5 °C to −2 °C.
(3) Short Beam Shear: The E-glass/epoxy laminates were characterized by a flat plateau in stress with increasing displacement after reaching maximum load whereas the carbon laminates exhibit decreasing stress capacity after maximum load. The carbon and E-glass laminates exhibited a 20% increase in short beam shear strength over the range from 20 °C to −2 °C.

5.2. Fracture performance

(1) Static Mode-I: Both of the E-glass and carbon laminates considered, exhibited a direct dependence of G_{IC} on

temperature with an observable trend that with decreasing temperature there was a corresponding decrease in G_{IC}. The E-glass laminates had a G_{IC} value of 1400 J/m^2 at −2 °C, which was 65% of the corresponding value at 20 °C, 2100 J/m^2.

(2) Dynamic Mode-I: The E-glass laminates exhibited higher critical strain energy release rates than the carbon laminates for dynamic Mode-I fracture. Additionally, the E-glass laminates displayed a larger dependence on temperature than did the carbon laminates. Finally, the observed dynamic Mode-I G_{ICd} values are significantly lower than the static Mode-I values.

5.3. Impact and flexure after impact strength performance

(1) Impact: The E-glass and carbon laminates show no significant dependence on impact behavior as a function of temperature in that the peak impact force is consistent across the temperature range considered in the study. However, the carbon laminates exhibit a brittle type behavior under impact loading whereas the E-glass laminates are more compliant during loading event.

(2) Flexure after impact: The four-point flexure after impact behavior of the E-glass laminate evaluated in the current study exhibits a trend in which the flexural strength decreases with increasing temperature with the specimens impacted at −2 °C having a larger residual strength than the samples impacted at 20 °C. There was no discernible trend found in the carbon laminates as the brittleness of the material under impact loading resulted in significant scatter in the results, even while the impact energy was consistent in all samples.

5.4. Dynamic Mechanical Analysis (DMA)

The linear viscoelastic behavior at small strains exhibit a matrix dominant behavior with a composite behavior at higher strain rates emerging for the carbon laminates at a lower strain level than for the E-glass laminates. The glass transition temperatures for the E-glass and carbon laminates are approximately 72 °C and 80 °C respectively. The mechanical properties of fiber-reinforced epoxy composites are essentially constant within the frequency ranges of interest in underwater acoustics.

The primary objective of the current manuscript was to present the meaningful findings pertaining to the mechanical and frequency dependent properties of carbon and E-glass laminates at temperatures of interest to the marine industry, specifically submerged vehicles. To further expand this breadth of knowledge, additional studies are warranted for low temperatures corresponding to structures exposed to low temperature air where the temperatures can be significantly lower than those of seawater.

Conflicts of interest

The authors declare that there is no conflicts of interest.

Acknowledgements

The financial support of the Naval Undersea Warfare Center (Division Newport) Internal Investment Program and In-House Laboratory Independent Research (ILIR) programs are gratefully acknowledged.

References

[1] D. Li, D. Fang, G. Zhang, H. Hu, Effect of temperature on bending properties and failure mechanism of three-dimensional braided composite, Mater. Des. 41 (2012) 167–170.
[2] S. Kichhannagari, Effects of Extreme Low Temperature on Composite Materials, University of New Orleans Theses and Dissertations, 2004. Paper 165.
[3] G. Springer, Environmental Effects on Composite Materials, Technomic Publishing Co, Inc., 1981.
[4] R.M. Jones, Mechanics of Composite Materials, Hemisphere Publishing Corp., 1975.
[5] J.C. Halpin, Primer on Composite Materials: Analysis, Technomic Publishing Co, Inc., 1984.
[6] V. Lopresto, I. Papa, A. Langella, Residual strength evaluation after impact tests in extreme temperature conditions. New equipment for CAI tests, Composites Part B 127 (2017) 44–52.
[7] I. Papa, A. Langella, V. Lopresto, Dynamic performances of basalt fibre laminates at room and low temperatures, Compos. Struct. 220 (2019) 652–661.
[8] Technical Reference Handbook, JPS Composite Materials, Anderson, SC. https://jpscm.com/wp-content/uploads/2017/10/2017-Data-Book-Small-1.pdf.
[9] ASTM D638-14, Standard Test Method for Tensile Properties of Plastics, ASTM International, West Conshohocken, PA, 2014. www.astm.org.
[10] ASTM D3410/D3410M-16, Standard Test Method for Compressive Properties of Polymer Matrix Composite Materials with Unsupported Gage Section by Shear Loading, ASTM International, West Conshohocken, PA, 2016. www.astm.org.
[11] ASTM D2344/D2344M-16, Standard Test Method for Short-Beam Strength of Polymer Matrix Composite Materials and Their Laminates, ASTM International, West Conshohocken, PA, 2016. www.astm.org.
[12] P. Cavallaro, Effects of weave styles and crimp gradients in woven kevlar/epoxy composites, Exp. Mech. 56 (2016) 617–635.
[13] ASTM D5528-13, Standard Test Method for Mode I Interlaminar Fracture Toughness of Unidirectional Fiber-Reinforced Polymer Matrix Composites, ASTM International, West Conshohocken, PA, 2013.
[14] T. Kusaka, M. Hojo, Y. Mai, T. Kurokawa, T. Nojima, S. Ochiai, Rate dependance of mode I fracture behavior in carbon-fibre/epoxy composite laminates, Compos. Sci. Technol. 58 (1998) 591–602.
[15] M. Rubinstein, R.H. Colby, Polymer Physics, Oxford University, Oxford, 2003.